Drying capacity of a continuous vibrated fluid bed dryer - Statistical and mechanistic model development

Wikstrom, Hakan

Elsevier B.V.
2023-10-15

Wikstrom, H, de Juan, L M, Remmelgas, J, Meier, R, Altmeyer, A, Emanuele, D, Jormanainen, M, Juppo, A & Tajarobi, P 2023, 'Drying capacity of a continuous vibrated fluid bed dryer - Statistical and mechanistic model development', International Journal of Pharmaceutics, vol. 645. https://doi.org/10.1016/j.ijpharm.2023.123368

http://hdl.handle.net/10138/590644
10.1016/j.ijpharm.2023.123368

Drying capacity of a continuous vibrated fluid bed dryer – Statistical and mechanistic model development

Håkan Wikström,[a] Luis Martin de Juan,[b] Johan Remmelgas,[c] Robin Meier,[d] Andreas Altmeyer,[d] Daniel Emanuele,[d] Miika Jormanainen,[e] Anne Juppo,[e] Pirjo Tajarobi[a,*]

[a] Early Product Development and Manufacturing, Pharmaceutical Sciences, BioPharmaceuticals R&D, AstraZeneca, Gothenburg, Sweden.

[b] Oral Product Development, Pharmaceutical Technology & Development, AstraZeneca, Gothenburg, Sweden.

[c] RCPE GmbH, Inffeldgasse 13/2, 8010 Graz, Austria

[d] L.B. Bohle Maschinen und Verfahren GmbH, Ennigerloh, Germany

[d] Division of Pharmaceutical Chemistry and Technology, University of Helsinki, Finland

* Corresponding author.
E-mail address: Pirjo.Tajarobi@astrazeneca.com

ABSTRACT

The drying capacity of a continuous vibrated fluid bed dryer was studied using a DoE by varying microcrystalline cellulose content in the formulation, water amount in the twin-screw granulation, inlet air temperature, air flow rate and the acceleration of the horizontal fluid-bed. Temperature and humidity profiles were measured along the dryer using wireless sensors. For the parameter space explored in this study, acceleration was the most influential process parameter of the dryer regarding the resulting granule moisture content. An empirical model was developed that allowed for fast and accurate moisture content prediction that could be incorporated into an enhanced control strategy. In addition, a mechanistic model was formulated that allow for prediction of temperature and moisture profiles, and most importantly the moisture content of the granules inside the dryer. The mechanistic model can be integrated to other unit operation models to provide overall understanding of an integrated continuous process line. The mechanistic model also makes it possible to define the equipment design requirements (e.g., length of the dryer) to meet the specific needs in terms of drying capacity, temperature and moisture profile.

GRAPHICAL ABSTRACT

<<GRAPHICS>>

Keywords: Continuous drying, vibrated fluid bed dryer, mechanistic model, digital twin, twin-screw wet granulation

1 INTRODUCTION

Continuous wet granulation is a common particle size enlargement step in pharmaceutical manufacturing. It is used to improve material flowability, homogeneity and tabletability, especially when the formulation cannot be tableted via direct compression (De Leersnyder et al. 2018; Dahlgren et al. 2019) and is always followed by a drying step. However, unlike continuous wet granulation, introduction of continuous drying of pharmaceutical granules has lagged behind continuous drying in chemical and food manufacturing. Implementation of continuous drying in the pharmaceutical industry was initially hindered by the inappropriate scale of the equipment, as well as the lack of a clear regulatory framework (Portier et al. 2021).

Until a few years ago, the most common method to dry wet granules in an integrated continuous manufacturing line was using a semi-continuous segmented fluid bed dryer (De Leersnyder et al. 2018; Pauli et al. 2019). Segmented fluid bed dryers operate by filling the multiple drying cells sequentially. After the drying cycle, the cells are emptied in the same order as they were filled, which ensures continuous operation (Vercruysse et al. 2013). Since the first cell is being emptied when the last cell is being filled, the drying time and the cell fill amount cannot be varied independently. This relationship between the cell fill amount and the drying time is a problem if it is found that the drying time is not sufficient because increasing the drying time then also increases the cell fill amount (unless the throughput is changed). Another challenge in segmented fluid bed dryers is related to the limited drying capacity due to the air flow capacity and drying time restriction (Randel et al. 2013; Dahlgren et al. 2019). That is because the air supply is divided between multiple drying segments operating in parallel compared to a batch-wise fluid bed dryer with only single drying chamber. This may cause insufficient granule drying especially with large and heavy granules with high moisture content. High drug load formulations could be potentially challenging, since they need high L/S ratios to achieve good flowability (Stauffer et al. 2019; Portier et al. 2020; Junnila et al. 2022).

In addition to the drying time being constrained by the cell fill amount, there is a constraint on the air flow rate through the different segments. In batch fluid bed drying, the air flow rate is sometimes decreased during drying to take into account the decrease in mass due to the loss of

moisture. In a segmented fluid dryer this is difficult to achieve since the different segments share a common air supply so that a decrease in the air flow rate affects all cells. In addition, since the actual mass of material differs between cells, the air flow rate between cells will also differ in such a way that cells with less material receive more air than filled cells, which is exactly opposite to what one would want. This problem can become even worse when the differential pressure over the product-filter differs from chamber to chamber. The resulting skewed air flow distribution can be a source of variability and can also decrease dryer efficiency, which is detrimental to the sustainability of the process.

Variability in the moisture content of the granules can also be caused by a difference in air temperature between the cells. Another challenge for a segmented fluid bed dryer is thus related to the variation in the air temperature between the cells (Grelier et al. 2022). The authors measured a difference in the air temperature of up to 5°C, which potentially impacts drying kinetics and the moisture content of the granules. Finally, the granule shape and size distribution may impair complete fluidization in segmented fluid bed dryers. In studies, the elongated granule shape or wide granule size distribution commonly seen in twin-screw wet granulation (TSWG) compared to the more spherical granules from batch high-shear wet granulation has resulted in insufficient drying due to channelling through the fluidized bed (Randel et al. 2013).

Other challenges in the development of continuous drying equipment for pharmaceutical use include the demanding requirements of a short, controllable and a narrow material residence time distribution, as well as clogging of the exhaust filters. While filter clogging is a challenge also for batch fluid bed drying, it is extra problematic for continuous drying since the filters need to be cleaned against a continuously incoming air stream or by stopping the process to remove, clean and replace them. Stopping the process obviously means that it cannot run continuously (De Leersnyder et al. 2018).

Recently equipment manufacturers have published novel and innovative continuous granule drying technologies such as spiral dryers, screw dryers and belt dryers. A spiral dryer is part of the Granuformer® powder-to-tablet line from Freund Vector, which features a spiral-shaped tube that dries the wet granules continuously (Freund Vector 2019). However, not

many studies with the dryer can be found. Lödige has developed a continuous dryer (GRANUCON® LCF) where a screw has been integrated in the fluid bed dryer. In addition, Zettl et al. (2021) described a continuous granule drying technology with a vacuum option in the form of a screw-designed dryer. The drying mechanism in this dryer is mainly conductive as the screw is internally heated while the possible vacuum enhances the drying capacity and enables the use of a lower drying temperature. As with the segmented fluid bed dryer, blockage of the exhaust air filters occurred with dusty material and the system generally requires further optimization (Zettl et al. 2021). Recently, a continuous horizontal vibrated fluid bed dryer (CFBD) was introduced for pharmaceutical use (Meier 2018; Elkhashap et al. 2019; Kiricenko and Kleinebudde, 2023; Franke et al. 2023). In such systems, the wet granules are transported via vibration along the bed, with only minor fluidization, while the hot air dries the granules.

Vibrated fluidized beds, which have been widely used in chemical and food industry, have several advantages compared to the conventional fluid bed dryers (Wang et al. 2003; Silva-Moris and Rocha, 2003; Palzer et al. 2007; Picado and Martínez 2012; Meili et al. 2012; Perazzini et al. 2017; Lehmann et al. 2019). For vertical vibrated fluidized beds, the minimum fluidization velocity and pressure drop is much lower leading to lower energy consumption compared with traditional fluid beds (Silva-Moris and Rocha, 2003; Meili et al. 2012; Perazzini et al. 2017; Lehmann et al. 2019). In the horizontal vibrated fluidized beds the residence time, the intensity of mixing and the heat and mass transfer properties can be controlled by changing the vibration parameters. Good conditions for heat and mass transfer can be ensured since the gas velocity and vibration parameters can be controlled independently. In addition, sticky materials, which normally are not fluidizable, can be processed.

While segmented fluid bed dryers have been studied to some degree, the literature on horizontal vibrated fluid bed dryers is considerably more sparse. The aim of this study was therefore to investigate the drying capacity of a continuous vibrated fluid bed dryer. This was accomplished by understanding the effect of formulation as well as TSWG and CFBD process variables on granule moisture content as well as granule size distribution using a commercial production scale Bohle QbCon-25 integrated powder-to-tablet manufacturing line. A DoE

comprising 84 placebo trials was performed with the aim to determine the suitability of a CFBD device for granules with varied moisture content, size distribution and composition. In order to understand the effect of the different process parameters on the studied granule properties, CFBD in-process information with multivariate analysis was used to determine the potential relationships.

2 MATERIAL AND METHODS

2.1 Materials

Three different placebo formulations consisting of mannitol, microcrystalline cellulose (MCC), 3% hydroxypropyl cellulose and 4% croscarmellose sodium were used in the study (Table 1). Depending on the formulation (P25, P50 and P75) the ratio between MCC and mannitol was varied 25:75, 50:50 and 75:25. Distilled water was used as the granulation liquid in all experiments.

2.2 Experimental methods

2.2.1 Twin-screw wet granulation

Granulation experiments were performed using an integrated continuous Bohle QbCon-25 manufacturing system (Figure 1) (L.B BohleMaschinen und Verfahren GmbH , Ennigerloh, Germany). A formulation pre-blend was fed with a loss-in-weight (LIW) feeder (Gericke DIW-PE-GZD-FB 200.22, Gericke AG, Regensdorf, Switzerland) to the feed segment of the twin-screw granulator (TSG) resulting in line rates from 10–20 kg/h. The screw configuration was unchanged during the whole experimental work. In the configuration, two kneading blocks consisting of two kneading elements (L=0.75D) with 60° offset angle separated by two conveying elements. The screw speed was kept constant at 400 rpm in all experiments. Distilled water was introduced in the barrel upstream of first kneading elements, via an integrated micro annular gear pump (MZR 7255, HNP Mikrosysteme, Schwerin, Germany). The liquid-to-solid (L/S) ratio was varied from 0.1-0.5 g/g according to the experimental plan (Table 2). Granules were collected during 3 minutes for each batch.

2.2.2 Continuous vibrated fluid bed drying

The granules were dried using an integrated continuous Bohle QbCon-25 vibrated fluid bed dryer. The function principle of QbCon-25 dryer is shown in Figure 2. The granules enter at

the inlet port, arriving from a TSG upstream of the dryer. The product then travels through the dryer and leaves it at the outlet port through a rotary valve. During the transition time through the dryer, the product comes into contact with hot and dry air that is supplied through the meshed bottom plate. Through the incoming air the granules get lightly fluidized. The transport through the dryer is induced by a controlled vibratory motion, which makes the traveling speed through the dryer almost completely independent of the air flowrate. The air leaves the system through the exhaust air zone of the dryer. To maintain a stable process and to prevent the air from flowing back to the TSG or even the powder feeder, which could cause process disturbances, the system features an inlet air and an outlet air system, to control the air flow and the direction of the air by a specified under-pressure within the product zone of the dryer. The total length of the CFBD used in this study was 150 cm.

2.2.3 Experimental plan

A two-part experimental design was used to better understand the drying performance of the vibrated fluid-bed dryer (Table 2). The first part was a 17-experiment central composite faced design with three centre points using the amount of MCC in the formulation, the line rate and the bed acceleration as the variables. Microcrystalline cellulose has a porous structure with both crystalline and amorphous regions and water can be absorbed both on the surfaces and penetrate the amorphous regions. MCC particles are able to hold large amounts of water inside the cellulose fibers, which results in less available water on the surfaces that can form liquid bridges (Luukkonen et al. 2001). Consequently, there is a linear correlation between the amount of MCC in the formulation and the water amount needed for the wet granulation (Chitu et al. 2011, Junnila et al. 2022). Hence, by varying the fraction of MCC, the amount of liquid that the formulation could take was also varied. In addition, the residence time and the bed thickness in the dryer were varied by changing the throughput and acceleration. This first part of the design was complemented with a 5-experiment full factorial design including one centre point to investigate the effect of the inlet air flow rate and temperature on the drying performance. The centre point of the central composite face-centered (CCF) design is also one corner of the full factorial design. In total these two designs resulted in 21 different experimental conditions, and at each of these conditions, the formulation was granulated using four different L/S ratios. In the low MCC formulation the L/S ratio was varied from 0.1 to 0.4

g/g, while the other formulations were granulated with L/S ratios from 0.2 to 0.5 g/g. Thus, the final experimental design consisted of 84 different experiments.

The wet granule moisture content (water amount) was varied by changing the L/S ratio as described above. The water-absorbing capacity of the material was varied by changing the MCC amount in the formulations (expressed as percent of fillers, 25–75%). The amount of material in the dryer was varied by changing line rate (10–20 kg/h). The residence time was varied by changing the acceleration (3.5–6.5 m/s^2) while the drying rate was varied by changing the inlet air temperature (77–93ºC) and air flow rate (240-314 Nm^3/h). The inlet air dew point was kept constant at -20ºC.

2.2.4 Process monitoring

The control system of the manufacturing line automatically collects in-process information such as inlet air temperature and humidity, exhaust air temperature and humidity, air flow rate, bed acceleration and granule temperature at the outlet of the dryer. The granule temperature was measured after the dryer using PT100 sensor (830-T2, Testo SE & Co. KGaA, Titisee-Neustadt, Germany). Additionally, Pyrobutton-TH sensors (OPULUS Ltd, Philadelphia, PA, USA) were used to measure both temperature and humidity in the dryer. The sensors can measure temperatures between -40 °C to +85 °C with a resolution of 0.0025 °C and calibrated accuracy of ± 0.1 °C. The relative humidity (RH) range is 0% to 100%RH with a resolution of 0.04% and a calibrated accuracy of ± 1.5%. A sampling rate of 1 s was used in all trials. A hanging bar was installed below the product filters (Figure 3). On this bar 8 sensors were placed equidistantly with a space of 16.5 cm between them. Furthermore, the distance from the centre of the sensor to the dryer bottom was set to 4 cm. For each experimental day a set of eight new sensors were installed. Finally, small Cubisens™ TC110 temperature sensors (CubeWorks, Ann Arbor, MI, USA) (1.7×3.9×2.2 mm) were used to measure the residence time in the dryer. The Cubisens sensors were dropped to the wet granules through the connection port between the TSG and the dryer. The temperature range of Cubisens sensors is 0 °C to 105 °C, the accuracy being ± 0.07 °C. One second sampling rate was used in the trials.

2.2.5 Moisture content of the granules

Loss on drying (LOD) measurements of the dried granules were performed with a moisture analyser (HR73-P Halogen Moisture Analyzer, Mettler Toledo GmbH, Greifensee,

Switzerland) in triplicate. The measurements were done at 110 ℃ using 4 g sample size until there was not further moisture loss, defined as less than 1 mg mass variation within 90 seconds.

2.2.6 Particle size distribution

The size distribution of dried granules was measured once for each batch with sieve analysis using a sieve shaker (Analysette 3 Vibratory Sieve Shaker, Fritsch GmbH, Idar-Oberstein, Germany) according to Ph. Eur (10.0, 2.9.38). The sample size used was 25 g. Granules were placed on top of the sieve tower during 5 min at an amplitude of 8 mm using a series of sieves (45, 90, 125, 180, 250, 355, 500, 710, 1000, 1400, 2000, 2800 and 4000 µm). The amount of retained granules on each sieve was weighed. Using the cumulative PSD from the sieve data, the DvX (d10, d50, d90) values were estimated by linear interpolation. The Sauter mean diameter (D_{32}) was also estimated from the distributions and included in the mechanistic model.

2.3 Modelling and data analysis

2.3.1 Statistical modelling

The experimental design was imported into MODDE 12 (MKS Instruments AB, Umeå, Sweden). The software was then used to assess the performance of the dryer by fitting the granule residual water content to the variables of experimental design using multiple linear regression.

2.3.2 One-dimensional plug flow model

Modelling of continuous vibrational fluid bed dryers have been previously discussed (Domokos et al. 2021; Elkhashap et al. 2019; Picado and Martinez, 2012). One-dimensional (1D) models are frequently used as part of system integrated models to simulate processes consisting of several unit operations to understand how the different process and material variables influence the critical quality attributes and process results with the aim to test, design and establish control strategies for processes to manufacture new products. These types of models represent a good compromise between the required level of detail on the predictions and the resources to generate and execute the models.

A 1D plug flow model has been proposed to describe the drying of particles in a vibrational fluid bed dryer. The main assumptions considered to describe the balance of moisture and energy in a differential of volume across the powder bed are the following:

1) The air flow is evenly distributed along the vibrated fluid bed.

2) The particles and the gas are well mixed within the differential volume (vertical and cross-sectional directions).

3) The particle size remains constant along the fluid bed dryer. There is no agglomeration, breakage or de-lumping.

4) The velocity of the granules along the dryer (or the mean residence time) is independent of the granule properties.

5) Axial dispersion of the particles can be neglected. The Peclet number calculated based on the residence time distribution curves in Elkhashap et al. (2019) is much larger than 100.

6) The bed porosity does not change along the dryer and does not depend on the formulation. A porosity of 70 % has been used in the simulations. Estimation of bed height and porosity is quite challenging using manufacturer recommendations of bed height below 1 cm. Based on extended literature on fluidized beds density (Kunii and Levenspiel 1991, Burgschweiger and Totsas 2002, Chen et al. 2017), bed porosity depends on operating parameters such as fluidization velocity and particle properties such as size distribution or. A correlation between model prediction errors and air flow rate is expected to provide an indication on whether this assumption holds for system considered in this study.

7) Heat losses and ambient temperature are constant for all the experiments considered. Ambient temperature is assumed to be 20 °C

Since moisture is stored in the granule but lost via its surface, it is appropriate to characterize the granule size distribution using a characteristic diameter that has the same proportion of surface to volume, this characteristic diameter is known as Sauter diameter. Equations (1)

through (4) are therefore based on a mass of particles having the same Sauter diameter as the granules in the experiments.

Equations representing the energy and mass balance to the particles in a differential of volume along the powder bed have been proposed. These can be written as a set of differential equations for the conservation of moisture and energy in the particle and gas phases. The mass balance for the particle phase can be written as

$$\rho_b bW(1-\varepsilon)\frac{dX}{dt} + \rho_b bW(1-\varepsilon)u_P\frac{dX}{dz} = -\frac{k_{zm}A_{ss}M_w\rho_b bW(1-\varepsilon)}{R}\gamma\left[\frac{p_{sat}}{T_P}\Big|_{T_P} f(X) - \frac{p_{sat}}{T_G}\Big|_{T_G}\varphi\right] \quad (1)$$

where X, ρ_B *and* A_{ss} are the dry-basis moisture content, particle density and specific surface area of the granules; W, b and ε are the width, height and porosity of the granule bed; M_w and R are the molecular weight of water and universal gas constant; P is the operating pressure, p_{sat} is the saturation vapor pressure of water, φ is the relative humidity and $f(X)$ represents the sorption isotherm. T_P and T_G represent the temperatures of particle ang gas phase. k_{zm} is the air-granule mass transfer coefficient. The conveying speed of the granules u_P has been estimated according to experimental data reported by Meier et al. (2018), Elkhashap et al. (2019) and Kiricenko and Kleinebudde (2023) for a QbCon®1. This vibrational fluid bed unit is a small scale of current unit. Equation (2) presents the dependence of the conveying speed as function of the vibration acceleration $A\omega$ and the surface air velocity u_a.

$$u_p = k_1 + k_2 A\omega + k_3 u_a \quad (2)$$

Coefficients in Equation 2 for different literature references are included in Table 3.

As indicated in Equation (1), the driving force for drying is assumed to be the difference in the molar concentration of water at the surface of a granule, $p_{sat}|_{T_P} f(X)/RT_p$, and in the bulk gas, $p_{sat}|_{T_G}\varphi/RT_G$. The saturation pressure of moisture in units of Torr is modelled according to Antoine equation,

$$\log p_{sat}(T) = A - \frac{B}{T+C} \quad (3)$$

In Equation 1, γ is a function that depends on the moisture content and accounts for the decrease in drying rate once the granule surface moisture has evaporated. Different bulk drying models are available to describe the drying kinetics of granules (Kemp, 2011; Fyhr and Kemp, 1998). All these models assume an initial constant drying rate period for moisture contents above a critical moisture content. During the so-called falling rate stage, the drying rate decreases according to an efficiency factor that, depending on the model, will adopt different shapes. In the present work, different expressions were considered including the described by Lyngberg et al. (2016), the reaction engineering approach (REA, Chen and Xie (1997) and the characteristic drying curve model (Langrish and Kockel 2001) that provided the most representative behaviour for our system.

The characteristic drying curve approach proposes a decay of the drying rate as a function of the relative difference between moisture content and the critical moisture content and it is expressed as

$$\gamma = \begin{cases} 1 & \text{for} \quad X \geq X_{cr} \\ \left(\frac{X_{cr}-X}{X_{cr}-X_{eq}}\right)^n & \text{for} \quad X < X_{cr} \end{cases} \tag{4}$$

where *n* is a model parameter.

The mass balance to water in the gas phase at a position *z* along the bed is defined as

$$\rho_A \varepsilon b W \frac{dY}{dt}\Big|_z + \frac{M_A}{L}(Y - Y_{in})\Big|_z = \frac{k_{zm} A_{ss} M_w \rho_B b W (1-\varepsilon)}{R} \gamma \left[\frac{p_{sat}}{T_P}\Big|_{T_P} f(X) - \frac{p_{sat}}{T_G}\Big|_{T_G} \varphi\right]\Big|_z \tag{5}$$

where Y_{in} and Y are the dry-basis moisture content of the air at the inlet to the dryer and at position *z* along the bed, ρ_A is the density of air, M_A is the inlet mass flow rate of dry air and L is the length of the vibrating bed.

The energy balance for the particle phase can be written

$$\rho_B b W (1-\varepsilon)(C_{PS} + X C_{PL}) \frac{dT_P}{dt} + \rho_B b W (1-\varepsilon)(C_{PS} + X C_{PL}) u_P \frac{dT_P}{dz} = h_m A_{SS} \rho_B b W (1 - \varepsilon)(T_G - T_P) - \frac{k_{xm} A_{ss} \rho_B b W (1-\varepsilon)}{P} \gamma \left[\frac{p_{sat}}{T_P}\Big|_{T_P} f(X) - \frac{p_{sat}}{T_G}\Big|_{T_G} \varphi\right] \Delta H_{vap}\Big|_{T_P} \tag{6}$$

where C_{PS} is the heat capacity of the solid, C_{PL} is the heat capacity of the liquid, h_m is the gas-granule heat transfer coefficient, and $\Delta H_{vap}\big|_{T_P}$ is the heat of vaporization at the particle temperature and h_m is the convective heat transfer coefficient between particle and gas. The energy balance for the gas phase at each position z along the dryer can be expressed as

$$\rho_A \varepsilon (C_{PA} + C_{PV} Y_{in}) \frac{dT_G}{dt}\Big|_z + \frac{M_A}{bwL}(C_{PA} + C_{PV} Y_{in})(T_G - T_{in})\Big|_z = -h_m A_{SS} \rho_B (T_G - T_P)|_z + \frac{k_{xm} A_{ss} \rho_B bW(1-\varepsilon)}{P} \gamma \left[\frac{p_{sat}}{T_P}\Big|_{T_P} f(X) - \frac{p_{sat}}{T_G}\Big|_{T_G} \varphi \right] C_{PV}(T_P - T_G)\Big|_z \quad (7)$$

where C_{PA} is the heat capacity of air, C_{PV} is the heat capacity of water vapor, and T_{in} is the inlet air temperature.

The first term on the left-hand sides of equations (1) and (5) through (7) represents water and energy accumulation in both phases that can be neglected under steady state conditions. The second term on the left-hand side of equations (1) and (5), represents convective transport of mass and energy in the granule phase while second term on the left-hand sides of equations (6) and (7) represent moisture uptake and energy loss of the gas as it flows through the bed. Terms that represent energy and mass transfer between gas and particles are included as the first term on the right-hand sides of equations (1) and (5) through (7). Lastly, the energy required to evaporate the water in the particle phase and the energy supplied by the gas phase are included as the second term on the right-hand sides of equations (6) and (7), respectively.

Different correlations for the particle-gas heat (h_m) and mass transfer coefficients (k_{zm}) have been proposed for fluidized beds (Kunii and Levenspiel 1991, Burgschweiger and Totsas 2002, Chen et al. 2017), and vibrational fluid bed dryers, see compilation by Picado and Martinez (2012). In the present work, different correlations proposed were evaluated in combination with different decaying rate functions γ as was indicated previously. Evaluation of the different combinations confirmed that the use Gunn's correlations (Gunn 1978) for the heat and mass transfer coefficients (expressed in terms of the Nusselt and Sherwood numbers) between gas and particle better described the observations in the current system. Picado and Martinez (2012) compilation showed differences on predicted heat transfer coefficients up to three orders of magnitude and concluded that heat and mass transfer coefficients for vibrated

fluid bed systems should be determined experimentally on the equipment focus of study. Gunn's correlations have been widely used for predicting heat and mass transfer coefficients on dense particle gas systems such as fluidized bed systems. These correlations can be written

$$Nu = \frac{h_m d_P}{k_G} = (7 - 10\varepsilon + 5\varepsilon^2)(1 + 0.7Re^{0.20}Pr^{0.33}) + (1.33 - 2.40\varepsilon + 1.20\varepsilon^2)Re^{0.70}Pr^{0.33} \quad (8)$$

$$Sh = \frac{k_{zm} d_P}{D_{VG}} = (7 - 10\varepsilon + 5\varepsilon^2)(1 + 0.7Re^{0.20}Sc^{0.33}) + (1.33 - 2.40\varepsilon + 1.20\varepsilon^2)Re^{0.70}Sc^{0.33} \quad (9)$$

where d_P is the particle diameter (Sauter mean diameter in present work), D_{VG} is the diffusivity of moisture in air, and ε is the bed porosity. According to these correlations the vibration acceleration and bed thickness have no influence on the heat and mass transfer coefficients, which are mainly controlled by the granule size and the relative velocity between the air and the granules.

The Reynolds, Prandtl and Schmidt number in equations (8) and (9) may be written as

$$Re = \frac{d_P u_a \rho_G}{\mu_G} \quad (10)$$

$$Pr = \frac{C_{PG}\mu_G}{k_G} \quad (11)$$

$$Sc = \frac{\mu_G}{\rho_G D_{VG}} \quad (12)$$

where μ_G is the gas viscosity, k_G is the gas thermal conductivity, and u_a is the gas superficial velocity.

The water sorption isotherm *f(X)* expresses the equilibrium relationships between moisture in the gas and the granule phases. There are different correlations in the literature to describe the sorption isotherm. The Henderson (Henderson, 1952) equation, which can be written

$$f(X) = 1 - e^{-kX^N} \quad (13)$$

has been used in the current model. Sorption isotherm parameters for any of the formulations considered in this study have been estimated based on the individual components' equilibrium data applying an additive approach as done by Godridge et al. (2005), Li et al. (2003) and Lewicki (1997). Based on the formulation space explored in this work, sorption isotherm parameters are a function of the relative amount of MCC in the formulation as described in Figure 4.

In order to account for the heat losses of the equipment, two additional equations have been implemented into the model (Figure 5): an equation for heat losses from the zone between the inlet temperature sensor and the powder bed, Q_{in},

$$Q_{in} = U_{in}A_{in}(T_{in} - T_{amb}) \quad (14)$$

and an equation for heat losses from the zone between powder bed and the position of the temperature and humidity sensor at the outlet, Q_{out}

$$Q_{out} = U_{out}A_{out}(T_{outlet} - T_{amb}) \quad (15)$$

It is assumed that these zones behave as a well mix systems and therefore the characteristic temperature of each zone is the exit temperature. During the evaluation of the model, it was concluded that heat losses at the outlet of the vibrational fluid bed may be neglected so that $U_{out}A_{out} = 0$ in order to improve the accuracy of temperature and relative humidity profiles along the bed.

The model described herein has been implemented in gProms Model Builder (Process Systems Enterprise, Siemens, London, United Kingdom).

3 RESULTS AND DISCUSSION

3.1 Data overview

The relevant formulation, process, sensor and characterisation data is shown in Supplementary information. As is evident from the data, the exhaust temperature and humidity are difficult to relate to process changes when running an experimental design in a continuous dryer. The reason being that the exhaust air is the collection of air coming from the first part of the bed to end (Figure 2). These values were compared to the values of the PyroButton sensor located at

the end of the dryer compartment (Figure 3). The data from this sensor is more representative of what would be expected based on the formulation and process changes, as well as the product temperature readings and LOD measurements.

3.2 Statistical model results

The variables of experimental design were fitted to the LOD of the dried granules using multiple linear regression, with the coefficient plot shown in Figure 6a. The resulting model showed excellent fit to the data as well as good predictability as evident from an R2 of 0.96 and a Q2 of 0.94. Additionally, the replicate plot indicates similar results from repeated experiments (Reproducibility of 0.997) as well as well distributed results over the experimental region, as evident in the replicate plot (Figure 6b).

As expected, the most influential factor affecting the granule residual water content was the L/S ratio. Moreover, not only a positive linear coefficient but also positive quadratic coefficient on the LOD response was identified for the L/S ratio. The quadratic effect of the L/S ratio is seen in the contour plots (Figure 7), as the LOD result increases more quickly with an increase in the L/S ratio at high (>0.35 g/g) L/S ratios compared to low L/S ratios. Additionally, the L/S ratio was non-linearly related to the LOD via an interaction with the line rate, which means that the L/S ratio becomes increasingly important when the line rate increases (Figure 6a). For the parameter space explored in this study, the acceleration was identified to be the most significant process parameter of the dryer that influenced granule moisture content (Figure 6a). Accordingly, higher acceleration values showed an increase in residual water content in dried granules, indicating that the material residence time in the continuous dryer has major effect on drying result.

The air flow rate and the inlet air temperature probably would have had greater impact on the LOD if these variables had been studied over a broader range as Kiricenko and Kleinebudde (2023) and Franke et al. (2023) did. However, the range of process parameters for this study were chosen based on the previous feasibility study, where it was observed that high air flow rates and inlet air temperatures were needed to dry these formulations, especially with high L/S ratios. By decreasing the acceleration, the residence time and thus the drying time were increased to facilitate an effective drying of the granules. The results are consistent with

Kiricenko and Kleinebudde (2023), who studied granule drying in the lab-scale CFBD (QbCon-1) dryer.

By changing the residence time of the product in the dryer via a change in the vibration speed at otherwise unmodified process parameters, the thickness of the granule bed changes because the hold-up mass changes. When increasing the vibration speed, the residence time decreases. The decrease in residence time leads to a shorter time for drying but at the same time to a reduced bed thickness and a higher ratio of available air per unit mass of product. A decrease in vibration speed shows the opposite effect: the residence time (i.e. the drying time) increases but the granule bed thickness increases. Consequently, two opposite effects compete with each other. However, the dryer was designed in such a way that the effect of the residence time should always be predominant in relevant process windows. This was supported by the experimental results, which showed that the effect of the change in residence time was predominant over the effect of changing granule layer thickness.

The contour plots of CFBD drying performance for different formulations are shown in Figure 7. The moisture content of the granules increased with increasing L/S ratio and generally decreased with increasing inlet air temperature. The increase in MCC amount in formulation resulted in an increase in granule residual water content (Figure 6a). As stated above, MCC is able to retain large quantities of water to itself, and the formulations with different amount of MCC interact with water in different way. Consequently, the initial moisture content in P50 and P75 formulation dry powder mixes were already higher as they contained relatively more hygroscopic MCC than P25 formulation, the initial moisture content of P50 formulation being 2%. The highest moisture contents for all formulations were seen when the fastest acceleration (6.5 m/s²) was used. However, at intense drying conditions (inlet air temperature: 93 °C, airflow rate: 314 Nm³/h and acceleration: 3.5 m/s²) it was possible to dry the granules to the initial moisture content of the powder blend (ca 2%) even with 0.5 g/g L/S ratio and 20 kg/h line rate.

Based on a previous feasibility study, it was decided not to push the dryer up to 25 kg/h or beyond 0.5 g/g L/S-ratio. However, if we extrapolate the Figure 7 the dryer should be able to dry the formulation to the same moisture level (2-3%) as the dry powder blend, even at a line rate of 25 kg/h. The effect of line rate on the bed height in the dryer is illustrated in Figure 8.

In spite of the differences in the thickness and the moisture content of the granule layer, good drying results were obtained for both batches. Nevertheless, thickness sensors would be beneficial from a process control point of view.

3.3 1D model results

The vibrational fluid bed dryer model proposed requires three parameters that have to be estimated experimentally: the heat transfer coefficient at the inlet of the equipment $U_{in}A_{in}$ (Equation 14) and the two characteristic drying curve parameters (Eq. 4), i.e., the critical moisture content X_{cr} and the exponential factor *n*. All the other model parameters have been measured and estimated from the equipment, operation and granule properties. Values of these parameters are summarized in Table 3.

The estimation of the model parameters $U_{in}A_{in}$, X_{cr}, and n has been done using the experiments described in Table 2. The algorithm for parameter estimation is based on Maximum Likelihood estimation. The experimental values used for this parameter estimation were the granule moisture (LOD) and the exhaust temperature for each experiment. The product temperature and exhaust relative humidity were not considered in the parameter estimation as both variables are dependent on granule moisture and exhaust temperature and their inclusion may lead to a worse parameter estimation resulting from effects such as an incorrect position of the probes or a lack of precision in certain measurements such as the inlet air flow rate. The estimated parameters are included in Table 3.

The LOD and exhaust temperature showed fair agreement between the predicted and observed values considering the number of estimated parameters and the variety of process conditions and formulation properties used during the tests. The mechanistic model presents the following evaluation metrics based on 64 experiments used for validation and 20 experiments used for parameter estimation: the LOD prediction has an RMSEv of 0.72% and a Q^2 of 0.78 whereas the exhaust temperature prediction has an RMSEv of 4.4 ºC and a Q^2 of 0.75. The mechanistic model performance metrics are worse than corresponding statistical model ones. However, a mechanistic model requires a much smaller dataset. Indeed, with only 5-10 experiments a good estimate can be obtained and increase in the number of experiments does not considerably improve the accuracy of the predictions.

A multivariate analysis of deviations in the LOD and exhaust temperature predictions revealed that the vibration acceleration was a critical factor that impacted the LOD estimation. However, the exhaust temperature prediction error was influenced mainly by the liquid to solid ratio and the particle diameter. The vibrational acceleration impacts the conveying speed of the granules and therefore the mean residence time distribution of the particles in the system. As indicated previously, the current assumptions use experimental data from QbCon®1 to assess the conveying speed in QbCon®25, butan analysis of error suggest that equation (2) may require further refinement in QbCon®25. The coefficients in equation (2) have been estimated based on current experiments resulting in an improved correlation (new estimated coefficients in Table 3) that reduced RMSEv in LOD to 0.59 and increased Q^2 to 0.85 (Figure 9). The predicted residence time agrees well with those obtained from using the Cubisens sensors, which suggested that it was around 40 s for the acceleration of 5 m/s^2 (Figure 10). The coefficient estimated for the influence of vibrational acceleration is more than two times higher than coefficient obtained by Kiricenko and Kleinebudde (2023) indicating that the properties of the granules used in this study are closer to those reported by Meier et al. (2018) and Elkhashap et al. (2019).

The prediction of the exhaust temperature is mainly impacted by the particle size of the granule and the liquid to solid ratio. Both parameters are correlated as typically a higher L/S ratio results in a larger particle size. It is proposed that the presence of lumps or poor distribution of granules during the initial part of the dryer influences the lack of accuracy of the model. These effects are expected to be more significant for L/S high ratios when product is typically more cohesive. Measurements indicate that the temperature over the powder bed is 10-15 ºC higher than the predicted temperature (Figure 9). This discrepancy is related to over prediction of heat and mass transfer on this specific position that would be related with a different initial particle size (e.g. lumps) or to a poorer distribution of product to what is assumed in the model. Formulations with high L/S ratios typically have lower exhaust temperatures and are therefore also affected more by this phenomenon. The particle size influences significantly the heat and mass transfer process, up to 20% deviations on particle size have been observed for replicates.

Other factors that influence the accuracy of the exhaust temperature prediction are the particle size and the thermal inertia during the experimental work. The variation in the model prediction is caused by the particle size distribution used to describe the granules; during experimental work three replicates of the same experiment reported a variation in the Sauter mean diameter of up to 20% that resulted in a difference in exhaust temperatures between simulations of up to 2 °C. Regarding the impact of thermal inertia, a constant heat loss during the whole experiments was assumed. The experimental work of 84 trials was executed over 3 days, and, although transition between points ensured that at least 3 residence times had passed between different experiments, the thermal inertia time scale may be larger between certain transitions.

The prediction of the product temperature and the relative humidity is included in Figure 9. The relative humidity at the exhaust depends on the exhaust temperature and the LOD estimations based on heat and mass balances to the unit. Therefore, the error in the prediction of the exhaust relative humidity is the accumulated error of both LOD and exhaust temperature estimation. The product temperature differs significantly from the measured value, especially when the product is dry at the exit of the system. Under these conditions, the product temperature is generally overpredicted relative to the measurement. A likely explanation for this overprediction could be the PT100 product temperature sensor position. Since the sensor was in a bucket outside the dryer, some granule cooling can be expected, especially as the granule temperature increases.

Predictions of air temperature and relative humidity profiles along the bed have been compared against data from the Pyrobutton sensors placed along the vibrated fluid bed dryer. Results of the predictions at different positions of the bed show good agreement with the experimental data, which implies that the model captures the overall drying mechanism correctly (Figure 11). Major discrepancies between model and experimental data are observed in the position of the first sensor where the temperature of the probe is consistently higher (10-15 °C) and, accordingly, the relative humidity is lower. As discussed previously, these discrepancies could be the result of lumps or an uneven distribution of product at this position that would result in a lower drying efficiency. It can be observed for the 0.5 L/S ratio that the model presents a higher variation across replicates than the actual data. This variation is

related to the particle size distribution, which is the only parameter that changes between simulations. An additional comparison between predicted and experimental results is included in Figure 12, with experiments that include a variation in MCC concentration, L/S ratio, vibration acceleration, air inlet flow rate and granule flow rate. Larger discrepancies are not related to any of these parameters specifically but are believed to be related to the particle size used in the model compared to the actual value.

Good agreement between the predicted temperature and humidity of the air above the powder bed justify the deviation of prediction of the product temperature because of position of the probe. Deviations between the predicted and actual product temperature result when operating under dried conditions. Under such conditions, the temperature of the air on the top of the bed is constant over the last proportion of the bed indicating that neither drying nor significant heat transfer to the granule occurs. This only can happen if the temperature of the air is close to the temperature of the granule.

This model provides an understanding of the relevance of the different operating parameters such as air flow rate, vibration acceleration, inlet temperature and throughput that can be used to define optimal conditions for operation to reduce CO_2 emissions. The model has been set up so that only three parameters must be estimated; the remaining parameters were estimated using standard characterization techniques. This significantly reduces the number of experiments required to drive predictions relative to the statistical model described in section 3.2.

3.4 Overall dryer performance

In this study the dryer was used for three days with varying particle sizes without any filter blockages. Since the material in the dryer is only lightly fluidized, there were no problems with the heavy, wet granules either.

Consequently, it is found that the continuous vibrated fluid-bed dryer offers several advantages over semi-continuous segmented dryers. Furthermore, the continuous vibrated fluid-bed dryer makes it possible to implement advanced process control for continuous wet granulation. The continuous vibrated fluid-bed dryer might even open up wet granulation as

an option for thermal and moisture labile drug substances as it exposes the drug substance to moisture and elevated temperatures for only a very short period of time.

Based on this study, it is possible to define a maximum capacity for a given vibrated fluid bed dryer and specify the dimensions required to achieve certain capacity, temperature and moisture requirements. Other applications of this model include assessments of advanced design features such as adding a cooling zone or stacking several beds to drive drying efficiency.

4 CONCLUSIONS

The drying capacity of a continuous vibrated fluid bed dryer was studied experimentally in a DoE by varying the MCC content in the formulation, the water amount in the twin-screw granulation, the inlet air temperature, the air flow rate and the acceleration of the fluid-bed. Temperature and humidity profiles were measured along the dryer using wireless sensors. A good statistical model was achieved for granule moisture content, which showed that for the parameter space explored in this study, acceleration was the most influential parameter for the granule moisture content of the studied drying process parameters. A mechanistic model was created which allows the prediction of temperature and moisture profiles, and most importantly the moisture content of the granules in the dryer. The predictions of this model were found to be in agreement with experimental data and require significantly fewer experiments. The mechanistic model can be integrated to other unit operation models to provide an overall understanding of the continuous process. The mechanistic model also makes it possible to define the equipment design requirements (e.g., length of the dryer) to meet the specific needs in terms of capacity, temperature, and moisture profile.

CREDIT AUTHORSHIP CONTRIBUTION STATEMENT

Håkan Wikström: Conceptualization, Methodology, Visualization, Writing – review & editing. **Luis Martin de Juan**: Conceptualization, Methodology, Writing – review & editing. **Johan Remmelgas**: Conceptualization, Methodology, Writing – review & editing. **Robin Meier**: Investigation, Writing – review & editing. **Andreas Altmeyer**: Investigation. **Daniel Emanuele**: Investigation **Miika Jormanainen**: Investigation, Writing – original draft, **Anne**

Juppo: Supervision, Writing – review & editing **Pirjo Tajarobi**: Conceptualization, Methodology, Supervision, Writing – original draft, Writing – review & editing.

ACKNOWLEDGEMENTS

The authors would like to acknowledge Lubomir Gradinarsky, Julie Bourquard and Josefine Lundsten (AZ) for the help with the CubiSens™ sensors. Emma Rooth and Lukas Dahlgren (AZ) are acknowledged for their help with the Pyrobutton sensors.

REFERENCES

Burgschweiger, J., Tsotsas, E., 2002. Experimental investigation and modelling of continuous fluidized bed drying under steady-state and dynamic conditions. Chem.Eng. Sci. 57, 5021 – 5038.

Chen, K., Bachmann, P., Bück, A., Jacob, M., Tsotsas, E. 2017. Experimental study and modeling of particle drying in a continuously-operated horizontal fluidized bed. Particuology, 34, 134-146.

Chitu, T., Oulahna, D., Hemati, M., 2011. Rheology, granule growth and granule strength: Application to the wet granulation of lactose–MCC mixtures. Powder Technol. 208, 441–453.

Dahlgren, G., Tajarobi, P., Simone, E., Ricart, B., Melnick, J., Puri, V., Stanton, C., Bajwa, G., 2019. Continuous Twin Screw Wet Granulation and Drying—Control Strategy for Drug Product Manufacturing. J. Pharm. Sci. 108(11), 3502–3514.

De Leersnyder, F., Vanhoorne, V., Bekaert, H., Vercruysse, J., Ghijs, M., Bostijn, N., Verstraeten, M., Cappuyns, P., Van Assche, I., Vander Heyden, Y., Ziemons, E., Remon, J.P., Nopens, I., Vervaet, C., De Beer, T., 2018. Breakage and drying behaviour of granules in a continuous fluid bed dryer: Influence of process parameters and wet granule transfer. Eur. J. Pharm. Sci. 115, 223–232.

Domokos, A., Pusztai, É., Madarász, L., Nagy, B., Gyürkés, M., Farkas, A., Fülöp, G., Casian, T., Szilágyi, B., Nagy, ZK. 2021. Combination of PAT and mechanistic modeling tools in a

fully continuous powder to granule line: Rapid and deep process understanding. Powder Technol. 388, 70–81. https://doi.org/10.1016/j.powtec.2021.04.059

Elkhashap, A., Meier, R., Abel, D., 2019. Modeling and control of a continuous vibrated fluidized bed dryer in pharmaceutical tablets production. Pharm.Ind. 81, 12, 1693-1700.

Franke, M., Riedel, T., Meier, R., Schmidt, C., Kleinebudde, P., 2023. Comparison of scale-up strategies in twin-screw wet granulation. Int.J.Pharm. 641, 123052.

Fyhr, C., Kemp, I., 1998. Comparison of different drying kinetics models for single particles, Drying Technology, 16 (7), 1339-1369, https://doi.org/10.1080/07373939808917465

Freund Vector: Granuformer R, 2018. Available at: https://www.freund-vector.com/wpcontent/uploads/2019/07/Using-Continuous-Granulation-to-Make-Robust-and-High-Drug-Load-APAP-Granules-Poster-2018.pdf (accessed 23 April, 2021).

Godridge, R.K., Bayly, A.E., Simmons, M.J.H., 2005. Moisture sorption isotherms of particulate mixtures. Proceedings of the 7th World Congress of Chemical Engineering, Glasgow, U.K., 1–10.

Grelier, A., Zadravec, M., Remmelgas, J., Forgber, T., Colacino, F., Pilcer, G., Stauffer, F., Hormann-Kincses, T., 2022. Model-Guided development of a semi-continuous drying process. Pharm.Res. 39:2005–2016. https://doi.org/10.1007/s11095-022-03361-4

Gunn, D.J. 1978 Transfer of heat and mass to particles in fixed and fluidized beds. Int. J. Heat Mass Transf. 21, 467-476.

Henderson, S.M., 1952. A basic concept of equilibrium moisture. Agricultural Engineering, 1952, 29-32.

Junnila, A., Wikström, H., Megarry, A., Gholami, A., Papathanasiou, F., Blomberg, A., Ketolainen, J., Tajarobi, P., 2022. Faster to First-time-in-Human: Prediction of the liquid solid ratio for continuous wet granulation. Eur.J.Pharm.Sci. 172, 106151.

Kemp, I., 2011. Drying Models, Myths, and Misconceptions. Chem. Eng. Technol. 34 (7), 1057–1066. DOI: 10.1002/ceat.201100061

Kiricenko, K., Kleinebudde, P., 2023. Drying behavior of a horizontal vibrated fluidized bed dryer for continuous manufacturing. Pharm.Technol.Dev. https://doi.org/10.1080/10837450.2023.2205932

Kunii, D., Levenspiel, O., 1991. Fluidization Engineering, 2nd Ed., Butterworth-Heinemann, Newton, US.

Langrish, T.A.G- and Kockel, T.G. 2001. The assessment of a characteristic drying curve for milk powder for use in computational fluid dynamics modelling. Chemical Engineering Journal. 84, 69-74.

Lehmann, S.E., Hartge, E.-U., Jongsma, A., deLeeuw, I.-M., Innings, F., Heinrich, S., 2019. Fluidization characteristics of cohesive powders in vibrated fluidized bed drying at low vibration frequencies. Powder Technol. 357, 54–63. doi.org/10.1016/j.powtec.2019.08.105

Lewicki, P., 1997. Water sorption isotherms and their estimation in food model mechanical mixtures. Journal of Food Engineering 32, 47-68.

Li, Y., Sanzgiri, Y., Chen. Y., 2003. A study on moisture isotherms of formulations: The use of polynomial equations to predict the moisture isotherms of tablet products. AAPS PharmSciTech 4(4), Article 59.

Lodige: Fluid bed dryer LCF for continuous operation, 2021. Available online: https://www.loedige.de/fileadmin/user_upload/GRANUCON_Continuous_Drying-201301.pdf (accessed on 10 April 2021)

Luukkonen, P., Maloney, T., Rantanen, J., Paulapuro, H., Yliruusi, J., 2001. Microcrystalline cellulose-water interaction – a novel approach using thermoporosimetry. Pharm. Res. 18 (11), 1562–1569.

Lyngberg, O., Bijnens, L., Geens, J., Marchut, A., Mehrman, S., Schafer, E., 2016. Applications of Modeling in Oral Solid Dosage Form Development and Manufacturing. In: Ierapetritou, M.G., Ramachandran, R. (eds) Process Simulation and Data Modeling in Solid Oral Drug Development and Manufacture. Methods in Pharmacology and Toxicology. Humana, New York, NY. https://doi.org/10.1007/978-1-4939-2996-2_1

Meier, R., Emanuele, D., 2018. Continuous wet granulation and fluid-bed drying – An experimental investigation of a new revolutionary system, https://www.continuous-production. com/images/QbCon_1/QbCon_1_continuous_drying.pdf.

Meier, R., Emanuele, D., Harbaum, P., 2020. Important elements in continuous granule drying processes - experiences from lab- and production-scale. TechnoPharm, Nr. 02, Seite 92.

Meili, L., Daleffe, R.V., Freire, J.T., 2012. Fluid dynamics of fluidized and vibrofluidized beds operating with Geldart C particles, Chem. Eng. Technol. 35, 1649–1656.

Palzer, S., 2007. Drying of wet agglomerates in a continuous fluid bed: Influence of residence time, air temperature and air-flow rate on the drying kinetics and the amount of oversize particles. Chem. Eng. Sci. 62, 463–470.

Pauli, V., Elbaz, F., Kleinebudde, P., Krumme, M., 2019. Orthogonal redundant monitoring of a new continuous fluid-bed dryer for pharmaceutical processing by means of mass and energy balance calculations and spectroscopic techniques. J. Pharm. Sci. 108, 2041–2055.

Perazzini, H., Freire, F.B., Freire, J.T., 2017. The influence of vibrational acceleration on drying kinetics in vibrofluidized bed. Chemical Engineering & Processing: Process Intensification 118, 124–130. http://dx.doi.org/10.1016/j.cep.2017.04.009

Green, D.W. and Perry, R.H. 2008 Perry’s Chemical Engineers’ Handbook.

Picado, A., Martínez, J. 2012. Mathematical modeling of a continuous vibrating fluidized bed dryer for grain. Drying Technology 30, 1469-1481.

Portier, C., Pandelaere, K., Delaet, U., Vigh, T., Di Pretoro, G., De Beer, T., Vervaet, C., Vanhoorne, V., 2020. Continuous twin screw granulation: A complex interplay between formulation properties, process settings and screw design. Int. J. Pharm. 576, 119004.

Portier, C., Vervaet, C., Vanhoorne, V., 2021. Continuous twin screw granulation: A review of recent progress and opportunities in formulation and equipment design. Pharmaceutics 13, 668. https://doi.org/10.3390/pharmaceutics13050668.

Randel, E., Schak, E., Islam, A., 2013. Fluid-bed dryers: Static versus vibrating. GEA Process Eng. 1–7.

Rehrl, J., Sacher, S., Horn, M., Khinast, J., 2020. End-point prediction of granule moisture in a ConsiGmaTM-25 segmented fluid bed dryer. Pharmaceutics, 12, 1–15.

Silva-Moris, V.A, Rocha, S.C.S., 2003. Development of a vibrofluidized bed and fluid-dynamic study with dry and wet adipic acid. Brazilian J.Chem.Eng. 20, 423 – 434.

Stauffer, F., Vanhoorne, V., Pilcer, G., Chavez, P.F., Vervaet, C., De Beer, T., 2019. Managing API raw material variability in a continuous manufacturing line—Prediction of process robustness. Int. J. Pharm. 569, 118525.

Vercruysse, J., Delaet, U., Van Assche, I., Cappuyns, P., Arata, F., Caporicci, G., De Beer, T., Remon, J.P., Vervaet, C., 2013. Stability and repeatability of a continuous twin screw granulation and drying system. Eur. J. Pharm. Biopharm. 85, 1031–1038.

Wang, X., Guo, Y., Shu, P., 2003. Numerical modelling of heat transfer between gas and solid in a vibrated fluidized bed, Appl. Therm. Eng. 23, 821–828.

Zettl, M., Aigner, I., Mannschott, T., Van Der Wel, P., Schrottner, H., Khinast, J., Krumme, M., 2021. Characterization of a novel drying technology for continuous processing of cohesive materials: An Ibuprofen Case Study. Org. Process Res. Dev. 25, 769–780.

Zhang, Y., Abatzoglou, N., 2022. Modelling of continuous drying of heat-sensitive pharmaceutical granules in a horizontal fluidised bed dryer combined with a screw conveyor at steady state. Chem.Eng.Sci. 255, 117678. https://doi.org/10.1016/j.ces.2022.117678

LIST OF TABLES

LIST OF FIGURES

Figure 12 **Model predictions (line) and experimental data (markers) of data profiles of temperature and humidity along the bed. Top graphs, impact of line rate: Formulation 25:75, L/S ratio: 0.3 g/g, air flow rate 314 Nm^3/h, inlet temperature 93 °C; line rate 10 kg/h (green, N1), 20 kg/h (red, N2). Mid graphs, impact of acceleration: Formulation 75:25, L/S ratio: 0.4 g/g, air flow rate 314 Nm^3/h, inlet temperature 93 °C, line rate 20 kg/h; acceleration 3.5 m/s^2 (blue, N6), 6.5 m/s^2 (orange, N8). Bottom graphs, impact of inlet temperature: Formulation 50:50, L/S ratio: 0.4 g/g, air flow rate 240 Nm^3/h, line rate 15 kg/h; inlet temperature 77 °C (purple, N18), 93 °C (grey, N20).**

TABLES

Table 1

Raw material	Vendor	Function	P25	P50	P75
Mannitol (Pearlitol 160C)	Roquette, Lestrem, France	Filler	69.7%	46.5%	23.3%
Microcrystalline cellulose (MCC), Avicel PH-102	Dupont, Cork, Ireland	Filler	23.3%	46.5%	69.7%
Hydroxypropyl cellulose (Klucel EXF)	Ashland Inc, Covington, KY, U.S.A.	Binder	3%	3%	3%
Croscarmellose (Ac-Di-Sol SD-711)	DuPont, Cork, Ireland	Disintegrant	4%	4%	4%

Table 2

Exp Name	MCC [%]	Flow rate [kg/h]	Liquid-solid ratio [ml/g]	Bed acceleration [m/s²]	Air flow rate [Nm3/h]	Inlet Temperature [°C]
N1	25	10	0.1, 0.2, 0.3, 0.4	3.5	314	93
N2	25	20	0.1, 0.2, 0.3, 0.4	3.5	314	93
N3	25	10	0.1, 0.2, 0.3, 0.4	6.5	314	93
N4	25	20	0.1, 0.2, 0.3, 0.4	6.5	314	93
N5	75	10	0.2, 0.3, 0.4, 05	3.5	314	93
N6	75	20	0.2, 0.3, 0.4, 05	3.5	314	93
N7	75	10	0.2, 0.3, 0.4, 05	6.5	314	93
N8	75	20	0.2, 0.3, 0.4, 05	6.5	314	93
N9	50	10	0.2, 0.3, 0.4, 05	5.0	314	93
N10	50	20	0.2, 0.3, 0.4, 05	5.0	314	93
N11	50	15	0.2, 0.3, 0.4, 05	3.5	314	93
N12	50	15	0.2, 0.3, 0.4, 05	6.5	314	93
N13	25	15	0.1, 0.2, 0.3, 0.4	5.0	314	93
N14	75	15	0.2, 0.3, 0.4, 05	5.0	314	93
N15	50	15	0.2, 0.3, 0.4, 05	5.0	314	93
N16	50	15	0.2, 0.3, 0.4, 05	5.0	314	93
N17	50	15	0.2, 0.3, 0.4, 05	5.0	314	93
N18	50	15	0.2, 0.3, 0.4, 05	5.0	240	77
N19	50	15	0.2, 0.3, 0.4, 05	5.0	314	77
N20	50	15	0.2, 0.3, 0.4, 05	5.0	240	93
N21	50	15	0.2, 0.3, 0.4, 05	5.0	277	85

Table 3

Parameter	Value	Unit
Granule particle density, ρ_B	650	kg/m^3
Granule specific surface area, A_{SS}	Calculated	m^2/kg
Granule heat capacity, C_{PS}	1300	J/kg K
Granule Sauter mean diameter, d_p	Measured	m
Granule critical moisture content, X_{cr}	71 ± 11	%
Exponential parameter of characteristic drying curve, n	1.89 ± 0.13	-
Air molar mass, M_G	0.029	kg/mol
Air density, ρ_A	calculated	kg/m^3
Air heat capacity, C_{PA}	1046	J/kg K
Air thermal conductivity, k_G	0.026	W/mK
Air viscosity, μ_G	2.0e-5	Pa s
Water molar mass, M_W	0.018	kg/mol
Water heat capacity, C_{PL}	4184	J/kg K
Water vapor heat capacity, C_{PV}	1912	J/kg K
Water diffusivity in air, D_{VG}	2.0e-5	m^2/s
Bed length, L	1.5	m
Bed width, w	0.24	m
Inlet overall heat transfer coefficoent, $U_{in}A_{in}$	10.5 ± 1.0	J/K
Exhaust overall heat tansfer coefficient, $U_{out}A_{out}$	0.0	J/K
Pressure, P	100 000	Pa
Ambient temperature, T_{amb}	20	ºC
Gas constant, R	8.314	J/K mol
Antoine equation, A	8.07131	-
Antoine equation, B	1730.630	ºC
Conveyance speed independent coefficient k_1 Elkhashap et al. (2019)	-0.0446	m/s

Kiricenko and Kleinebudde (2023) Estimation based on this study data.	-0.014 -0.057 ± 0.018	
Conveyance speed, vibrational acceleration coefficient, k_2 Elkhashap et al. (2019) Kiricenko and Kleinebudde (2023) Estimation based on this study data.	 0.0091 0.0037 0.009 ± 0.002	s
Conveyance speed, air superficial velocity coefficient, k_3 Elkhashap et al. (2019) Kiricenko and Kleinebudde (2023) Estimation based on this study data.	 0.12 0.0632 0.13 ± 0.06	-

FIGURES

Figure 1

Figure 2

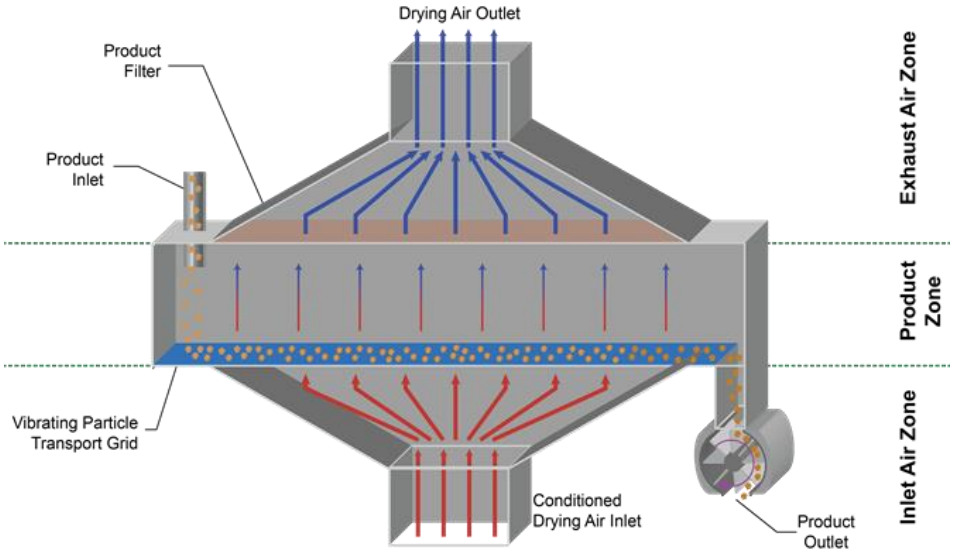
Drying Air Outlet
Product Filter
Product Inlet
Exhaust Air Zone
Product Zone
Inlet Air Zone
Vibrating Particle Transport Grid
Conditioned Drying Air Inlet
Product Outlet

Figure 3

Figure 4

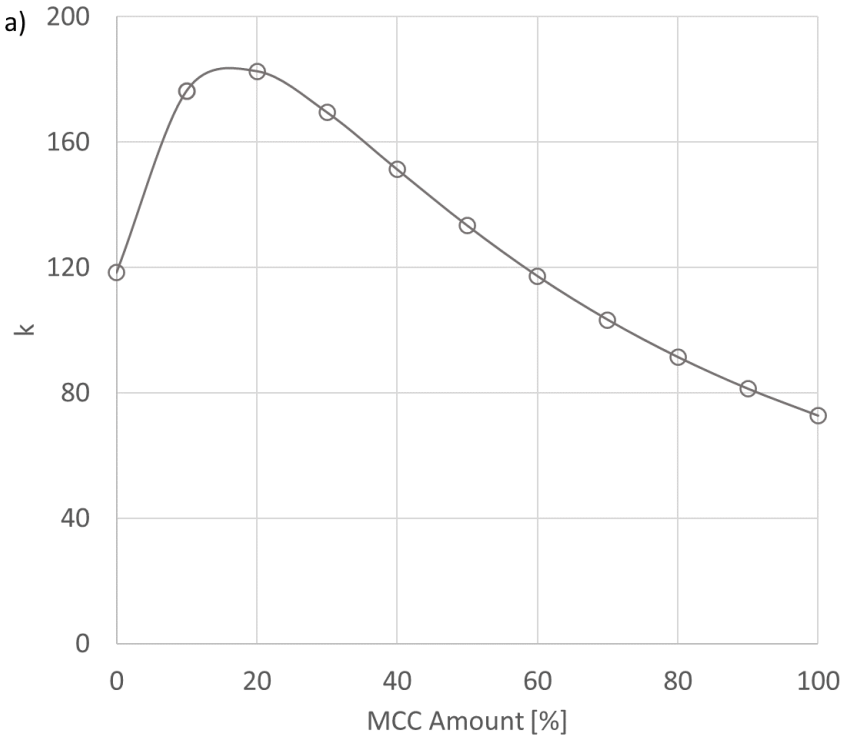
a)
200
160
120
80
40
0
k
0
20
40
60
80
100
MCC Amount [%]

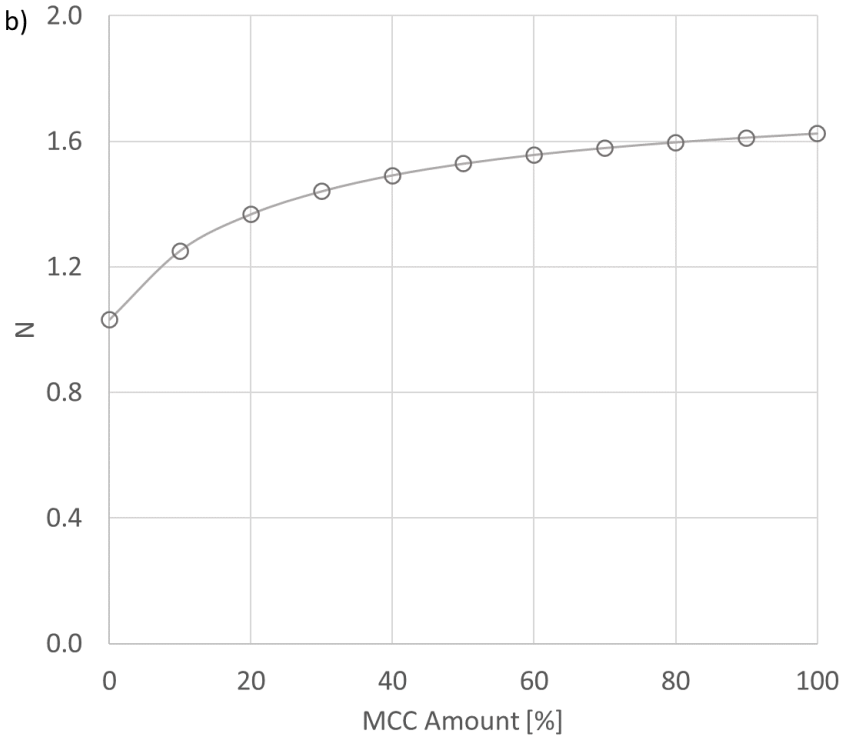
b)
2.0
1.6
1.2
0.8
0.4
0.0
N
0
20
40
60
80
100
MCC Amount [%]

Figure 5

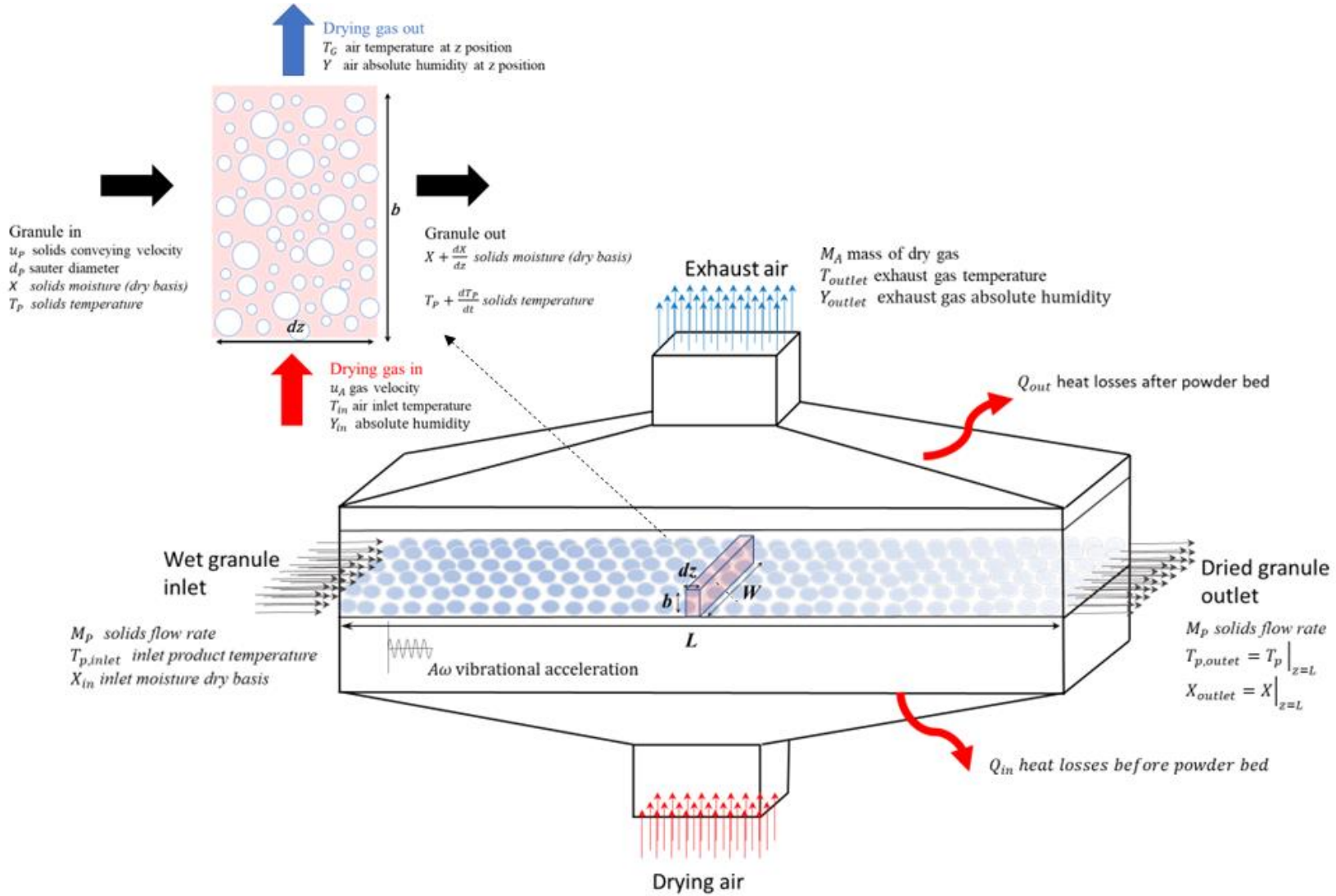
Drying gas out
T_G air temperature at z position
Y air absolute humidity at z position
Granule in
u_p solids conveying velocity
d_p sauter diameter
X solids moisture (dry basis)
T_p solids temperature
b
dz
Granule out
$X + \frac{dX}{dz}$ solids moisture (dry basis)
$T_p + \frac{dT_p}{dt}$ solids temperature
Drying gas in
u_A gas velocity
T_{in} air inlet temperature
Y_{in} absolute humidity
Exhaust air
M_A mass of dry gas
T_{outlet} exhaust gas temperature
Y_{outlet} exhaust gas absolute humidity
Q_{out} heat losses after powder bed
Wet granule inlet
M_p solids flow rate
$T_{p,inlet}$ inlet product temperature
X_{in} inlet moisture dry basis
dz
b
W
L
$A\omega$ vibrational acceleration
Dried granule outlet
M_p solids flow rate
$T_{p,outet} = T_p|_{z=L}$
$X_{outlet} = X|_{z=L}$
Q_{in} heat losses before powder bed
Drying air

Figure 6

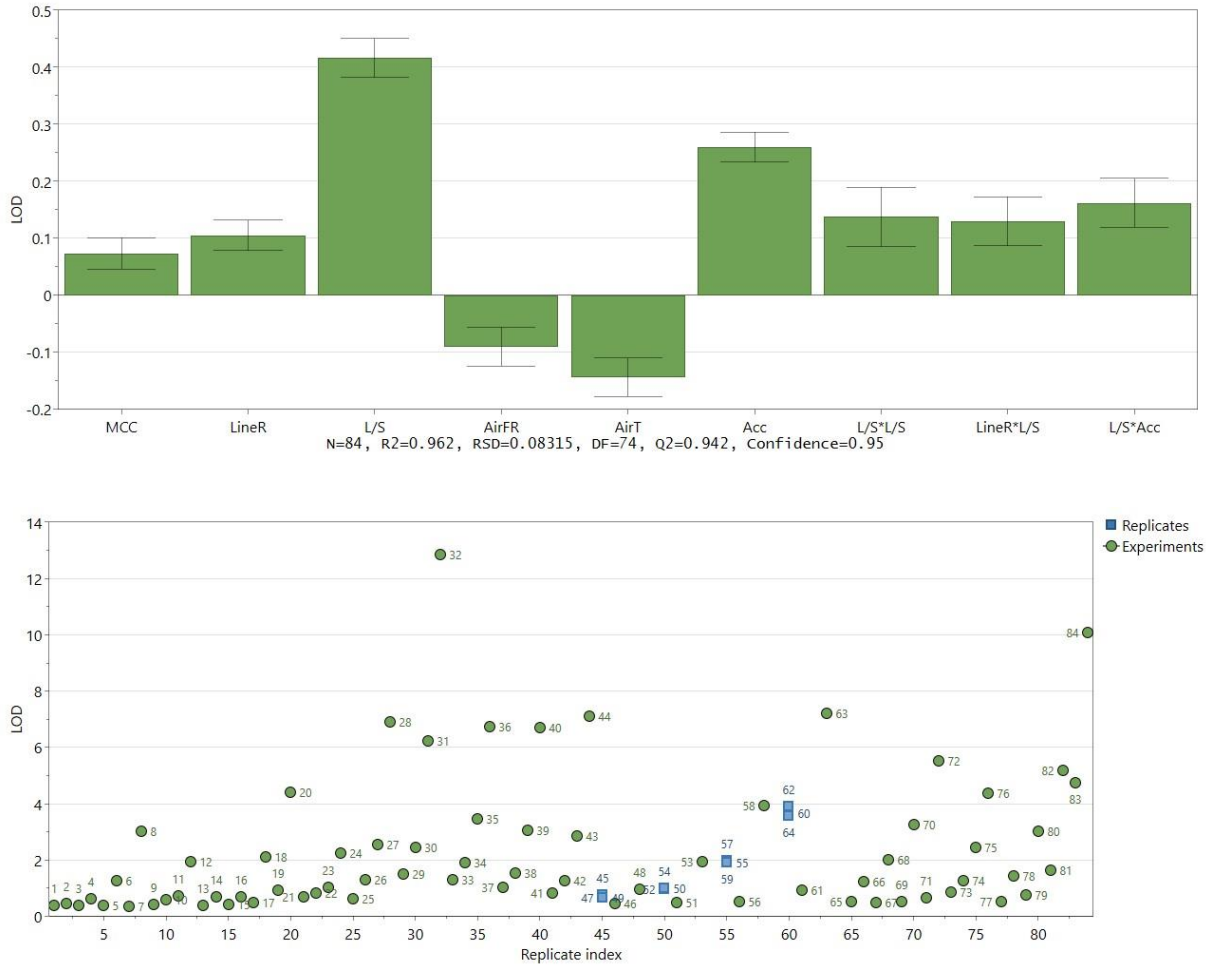
LOD
MCC
LineR
L/S
AirFR
AirT
Acc
L/S*L/S
LineR*L/S
L/S*Acc
N=84, R2=0.962, RSD=0.08315, DF=74, Q2=0.942, Confidence=0.95
Replicates
Experiments
Replicate index

Figure 7

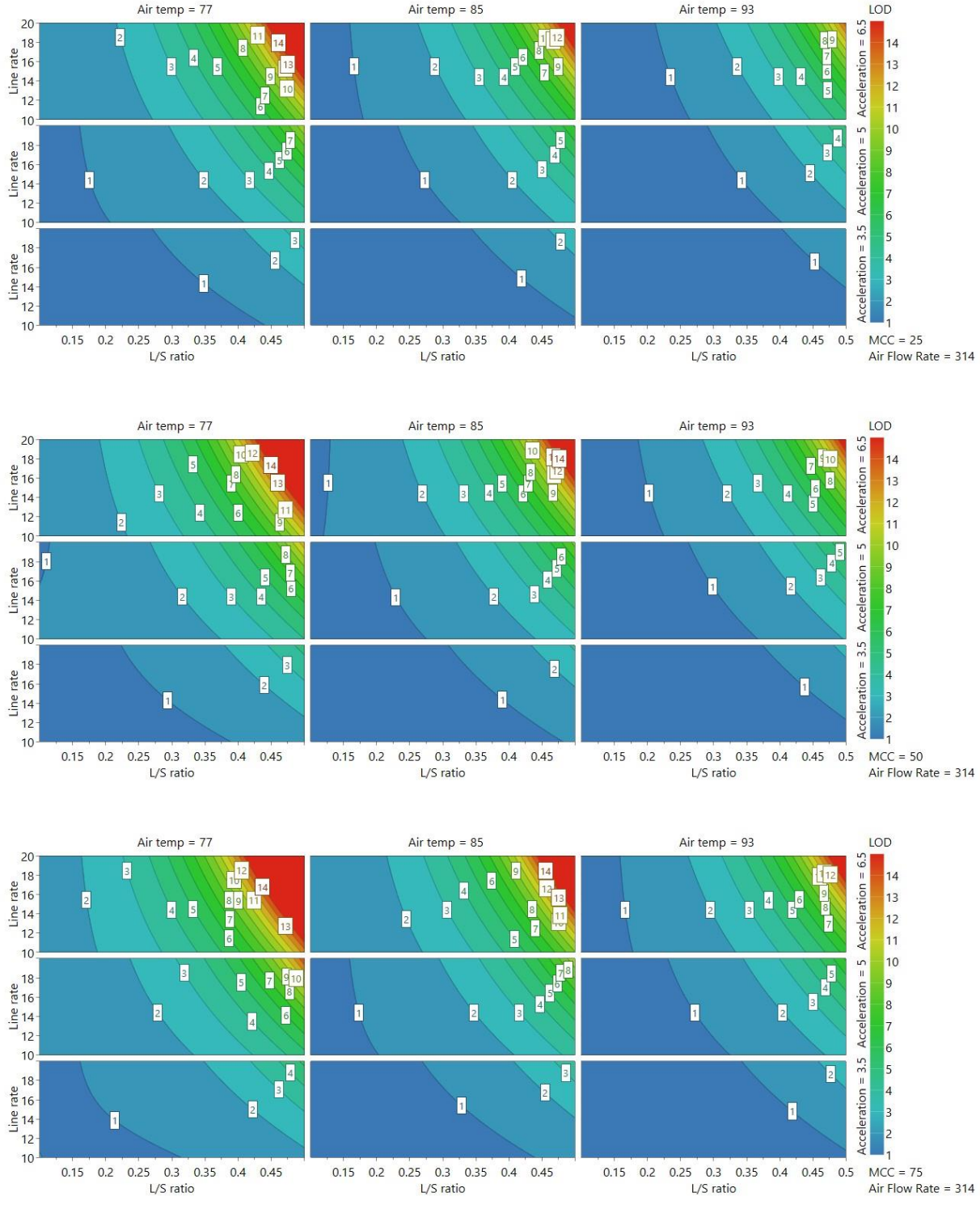
Air temp = 77
Air temp = 85
Air temp = 93
LOD
Line rate
L/S ratio
Acceleration = 6.5
Acceleration = 5
Acceleration = 3.5
MCC = 25
Air Flow Rate = 314
MCC = 50
Air Flow Rate = 314
MCC = 75
Air Flow Rate = 314

Figure 8

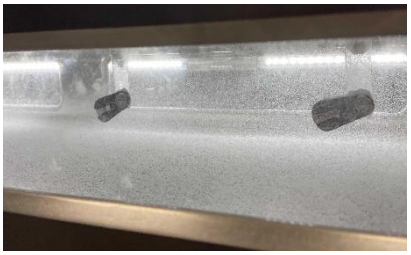

Figure 9

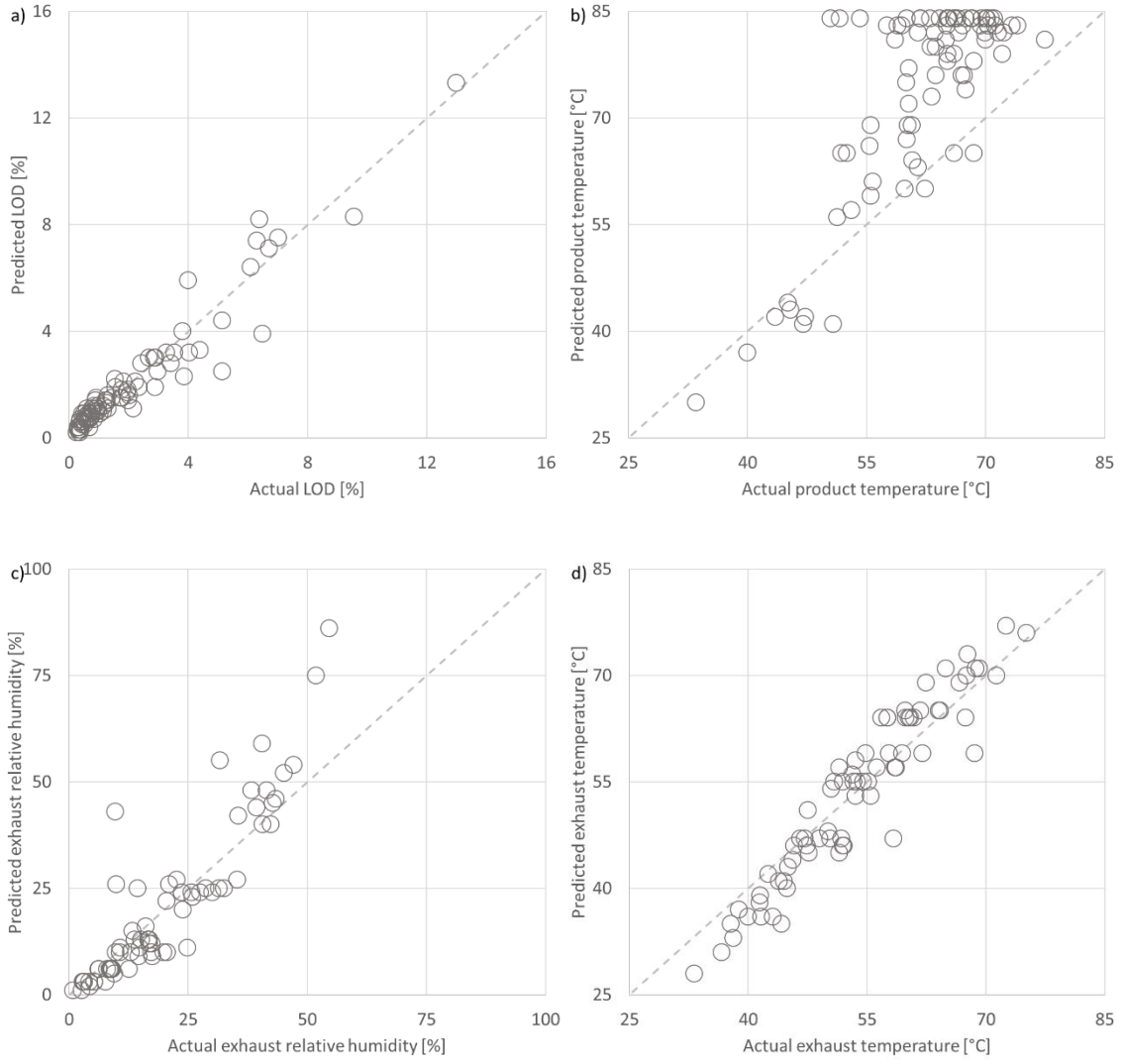
a)
Predicted LOD [%]
Actual LOD [%]
0
4
8
12
16
b)
Predicted product temperature [°C]
Actual product temperature [°C]
25
40
55
70
85
c)
Predicted exhaust relative humidity [%]
Actual exhaust relative humidity [%]
0
25
50
75
100
d)
Predicted exhaust temperature [°C]
Actual exhaust temperature [°C]

Figure 10

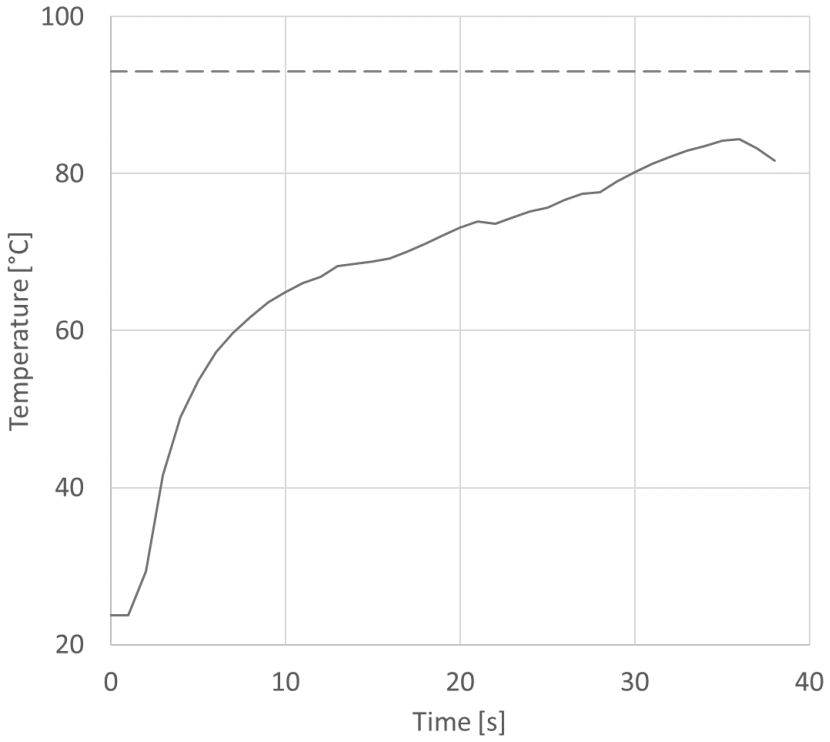

Figure 11

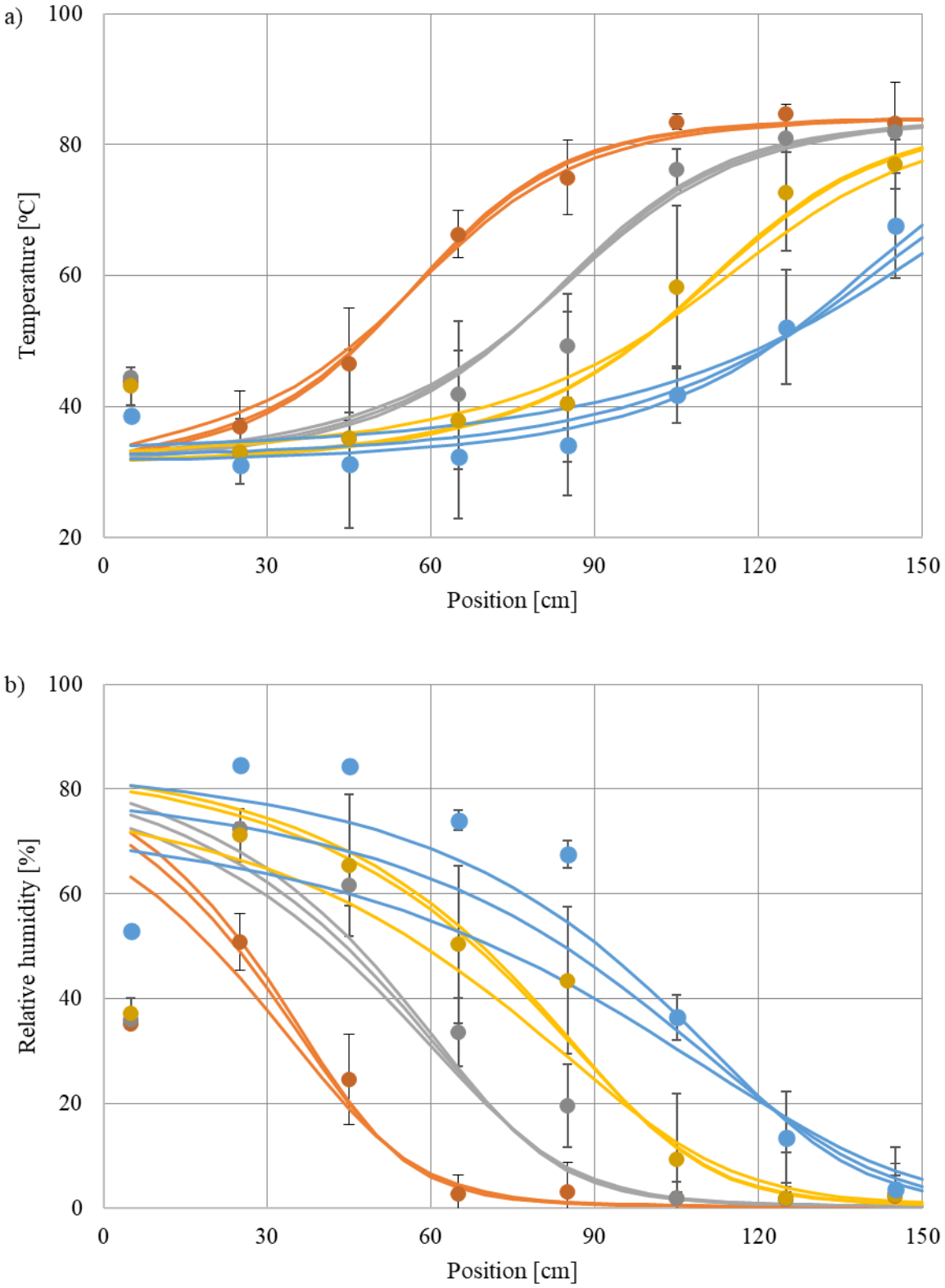
a)
Temperature [ºC]
Position [cm]
b)
Relative humidity [%]
Position [cm]

Figure 12

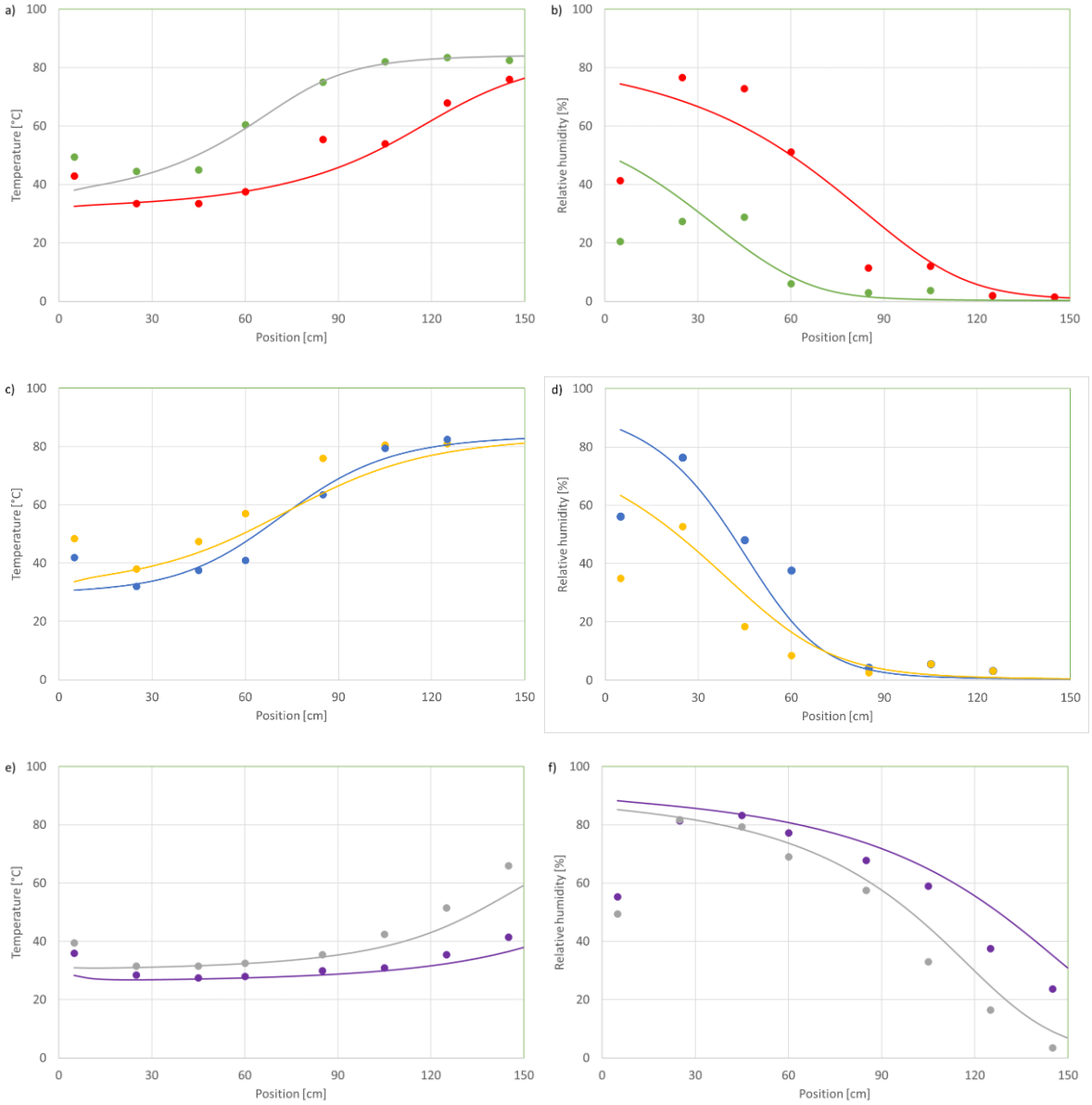
a)
Temperature [°C]
Position [cm]
b)
Relative humidity [%]
Position [cm]
c)
Temperature [°C]
Position [cm]
d)
Relative humidity [%]
Position [cm]
e)
Temperature [°C]
Position [cm]
f)
Relative humidity [%]
Position [cm]